Search for R-parity violation with a $\bar{U}\bar{D}\bar{D}$ coupling at $\sqrt{s}$ = 189 GeV

P. Abreu, W. Adam, T. Adye, P. Adzic, I. Azhinenko, Z. Albrecht, T. Alderweireld, G.D. Alekseev, R. Alemany, T. Allmendinger, et al.

EUROPEAN ORGANIZATION FOR NUCLEAR RESEARCH

CERN–EP/2000-127

16 August 2000

Search for R-parity violation with a $\bar{U}\bar{D}\bar{D}$ coupling at $\sqrt{s} = 189$ GeV

DELPHI Collaboration

Abstract

Searches for pair production of gauginos and squarks in e^+e^- collisions at a centre-of-mass energy of 189 GeV have been performed on data corresponding to an integrated luminosity of 158 pb^{-1} collected by the DELPHI detector at LEP. The data were analyzed under the assumption of non-conservation of R-parity through a single dominant $\bar{U}\bar{D}\bar{D}$ coupling between squarks and quarks. Typical final states contain between 4 and 10 jets with or without additional leptons. No excess of data above Standard Model expectations was observed. The results were used to constrain domains of the MSSM parameter space and derive limits on the masses of supersymmetric particles.
The following mass limits at 95% CL were obtained from these searches:

- neutralino mass: $m_{\tilde{\chi}_1^0} \geq 32$ GeV
- chargino mass: $m_{\tilde{\chi}_1^+} \geq 94$ GeV
- stop and sbottom mass (indirect decay) with $\Delta M > 5$ GeV:
  $m_{\tilde{t_1}} \geq 74$ GeV, for $\Phi_{mix} = 0$ rad
  $m_{\tilde{t_1}} \geq 59$ GeV, for $\Phi_{mix} = 0.98$ rad
  $m_{\tilde{b_1}} \geq 72$ GeV, for $\Phi_{mix} = 0$ rad.

The angle ϕ_{mix} is the mixing angle between left and right handed quarks.

(To be submitted to Physics Letters B)

P.Abreu[22], W.Adam[52], T.Adye[38], P.Adzic[12], I.Ajinenko[44], Z.Albrecht[18], T.Alderweireld[2], G.D.Alekseev[17], R.Alemany[51], T.Allmendinger[18], P.P.Allport[23], S.Almehed[25], U.Amaldi[29], N.Amapane[47], S.Amato[49], E.G.Anassontzis[3], P.Andersson[46], A.Andreazza[9], S.Andringa[22], P.Antilogus[26], W-D.Apel[18], Y.Arnoud[9], B.Åsman[46], J-E.Augustin[26], A.Augustinus[9], P.Baillon[9], A.Ballestrero[47], P.Bambade[20], F.Barao[22], G.Barbiellini[48], R.Barbier[26], D.Y.Bardin[17], G.Barker[18], A.Baroncelli[40], M.Battaglia[16], M.Baubillier[24], K-H.Becks[54], M.Begalli[6], A.Behrmann[54], P.Beilliere[8], Yu.Belokopytov[9], N.C.Benekos[33], A.C.Benvenuti[5], C.Berat[15], M.Berggren[24], D.Bertrand[2], M.Besancon[41], M.S.Bilenky[17], M-A.Bizouard[20], D.Bloch[10], H.M.Blom[32], M.Bonesini[29], M.Boonekamp[41], P.S.L.Booth[23], G.Borisov[20], C.Bosio[43], O.Botner[50], E.Boudinov[32], B.Bouquet[20], C.Bourdarios[20], T.J.V.Bowcock[23], I.Boyko[17], I.Bozovic[12], M.Bozzo[14], M.Bracko[45], P.Branchini[40], R.A.Brenner[50], P.Bruckman[9], J-M.Brunet[8], L.Bugge[34], T.Buran[34], B.Buschbeck[52], P.Buschmann[54], S.Cabrera[51], M.Caccia[28], M.Calvi[29], T.Camporesi[9], V.Canale[39], F.Carena[9], L.Carroll[23], C.Caso[14], M.V.Castillo Gimenez[51], A.Cattai[9], F.R.Cavallo[5], V.Chabaud[9], Ph.Charpentier[9], P.Checchia[37], G.A.Chelkov[17], R.Chierici[47], P.Chliapnikov[9,44], P.Chochula[7], V.Chorowicz[26], J.Chudoba[31], K.Cieslik[19], P.Collins[9], R.Contri[14], E.Cortina[51], G.Cosme[20], F.Cossutti[9], M.Costa[51], H.B.Crawley[1], D.Crennell[38], S.Crepe[15], G.Crosetti[14], J.Cuevas Maestro[35], S.Czellar[16], M.Davenport[9], W.Da Silva[24], G.Della Ricca[48], P.Delpierre[27], N.Demaria[47], A.De Angelis[48], W.De Boer[18], C.De Clercq[2], B.De Lotto[48], A.De Min[37], L.De Paula[49], H.Dijkstra[9], L.Di Ciaccio[9,39], J.Dolbeau[8], K.Doroba[53], M.Dracos[10], J.Drees[54], M.Dris[33], A.Duperrin[26], J-D.Durand[9], G.Eigen[4], T.Ekelof[50], G.Ekspong[46], M.Ellert[50], M.Elsing[9], J-P.Engel[10], M.Espirito Santo[9], G.Fanourakis[12], D.Fassouliotis[12], J.Fayot[24], M.Feindt[18], J.Fernandez[42], A.Ferrer[51], E.Ferrer-Ribas[20], F.Ferro[14], S.Fichet[24], A.Firestone[1], U.Flagmeyer[54], H.Foeth[9], E.Fokitis[33], F.Fontanelli[14], B.Franek[38], A.G.Frodesen[4], R.Fruhwirth[52], F.Fulda-Quenzer[20], J.Fuster[51], A.Galloni[23], D.Gamba[47], S.Gamblin[20], M.Gandelman[49], C.Garcia[51], C.Gaspar[9], M.Gaspar[49], U.Gasparini[37], Ph.Gavillet[9], E.N.Gazis[33], D.Gele[10], T.Geralis[12], L.Gerdyukov[44], N.Ghodbane[26], I.Gil[51], F.Glege[54], R.Gokieli[9,53], B.Golob[9,45], G.Gomez-Ceballos[42], P.Goncalves[22], I.Gonzalez Caballero[42], G.Gopal[38], L.Gorn[1], Yu.Gouz[44], V.Gracco[14], J.Grahl[1], E.Graziani[40], P.Gris[41], G.Grosdidier[20], K.Grzelak[53], J.Guy[38], C.Haag[18], F.Hahn[9], S.Hahn[54], S.Haider[9], A.Hallgren[50], K.Hamacher[54], J.Hansen[34], F.J.Harris[36], F.Hauler[18], V.Hedberg[9,25], S.Heising[18], J.J.Hernandez[51], P.Herquet[2], H.Herr[9], J.-M.Heuser[54], E.Higon[51], S-O.Holmgren[46], P.J.Holt[36], S.Hoorelbeke[2], M.Houlden[23], J.Hrubec[52], M.Huber[18], G.J.Hughes[23], K.Hultqvist[9,46], J.N.Jackson[23], R.Jacobsson[9], P.Jalocha[19], R.Janik[7], Ch.Jarlskog[25], G.Jarlskog[25], P.Jarry[41], B.Jean-Marie[20], D.Jeans[36], E.K.Johansson[46], P.Jonsson[26], C.Joram[9], P.Juillot[10], L.Jungermann[18], F.Kapusta[24], K.Karafasoulis[12], S.Katsanevas[26], E.C.Katsoufis[33], R.Keranen[18], G.Kernel[45], B.P.Kersevan[45], Yu.Khokhlov[44], B.A.Khomenko[17], N.N.Khovanski[17], A.Kiiskinen[16], B.King[23], A.Kinvig[23], N.J.Kjaer[9], O.Klapp[54], H.Klein[9], P.Kluit[32], P.Kokkinias[12], V.Kostioukhine[44], C.Kourkoumelis[3], O.Kouznetsov[17], M.Krammer[52], E.Kriznic[45], Z.Krumstein[17], P.Kubinec[7], J.Kurowska[53], K.Kurvinen[16], J.W.Lamsa[1], D.W.Lane[1], V.Lapin[44], J-P.Laugier[41], R.Lauhakangas[16], G.Leder[52], F.Ledroit[15], V.Lefebure[2], L.Leinonen[46], A.Leisos[12], R.Leitner[31], G.Lenzen[54], V.Lepeltier[20], T.Lesiak[19], M.Lethuillier[41], J.Libby[36], W.Liebig[54], D.Liko[9], A.Lipniacka[9,46], I.Lippi[37], B.Loerstad[25], J.G.Loken[36], J.H.Lopes[49], J.M.Lopez[42], R.Lopez-Fernandez[15], D.Loukas[12], P.Lutz[41], L.Lyons[36], J.MacNaughton[52], J.R.Mahon[6], A.Maio[22], A.Malek[54], T.G.M.Malmgren[46], S.Maltezos[33], V.Malychev[17], F.Mandl[52], J.Marco[42], R.Marco[42], B.Marechal[49], M.Margoni[37], J-C.Marin[9], C.Mariotti[9], A.Markou[12], C.Martinez-Rivero[20], S.Marti i Garcia[9], J.Masik[13], N.Mastroyiannopoulos[12], F.Matorras[42], C.Matteuzzi[29], G.Matthiae[39], F.Mazzucato[37], M.Mazzucato[37], M.Mc Cubbin[23], R.Mc Kay[1], R.Mc Nulty[23], G.Mc Pherson[23], C.Meroni[28], W.T.Meyer[1], E.Migliore[9], L.Mirabito[26], W.A.Mitaroff[52], U.Mjoernmark[25], T.Moa[46], M.Moch[18], R.Moeller[30], K.Moenig[9,11], M.R.Monge[14], D.Moraes[49], X.Moreau[24], P.Morettini[14], G.Morton[36], U.Mueller[54], K.Muenich[54], M.Mulders[32], C.Mulet-Marquis[15], R.Muresan[25], W.J.Murray[38], B.Muryn[19], G.Myatt[36], T.Myklebust[34], F.Naraghi[15], M.Nassiakou[12], F.L.Navarria[5], K.Nawrocki[53], P.Negri[29], N.Neufeld[9], R.Nicolaidou[41], B.S.Nielsen[30], P.Niezurawski[53], M.Nikolenko[10,17], V.Nomokonov[16], A.Nygren[25], V.Obraztsov[44], A.G.Olshevski[17], A.Onofre[22], R.Orava[16], G.Orazi[10], K.Osterberg[16], A.Ouraou[41], A.Oyanguren[51], M.Paganoni[29], S.Paiano[5], R.Pain[24], R.Paiva[22], J.Palacios[36], H.Palka[19], Th.D.Papadopoulou[9,33], L.Pape[9], C.Parkes[9], F.Parodi[14], U.Parzefall[23], A.Passeri[40], O.Passon[54], T.Pavel[25], M.Pegoraro[37], L.Peralta[22], M.Pernicka[52], A.Perrotta[5], C.Petridou[48], A.Petrolini[14], H.T.Phillips[38], F.Pierre[41], M.Pimenta[22], E.Piotto[28], T.Podobnik[45], M.E.Pol[6], G.Polok[19], P.Poropat[48], V.Pozdniakov[17], P.Privitera[39], N.Pukhaeva[17], A.Pullia[29], D.Radojicic[36], S.Ragazzi[29], H.Rahmani[33], J.Rames[13], P.N.Ratoff[21], A.L.Read[34], P.Rebecchi[9], N.G.Redaelli[29], M.Regler[52], J.Rehn[18], D.Reid[32], P.Reinertsen[4], R.Reinhardt[54], P.B.Renton[36], L.K.Resvanis[3], F.Richard[20], J.Ridky[13], G.Rinaudo[47], I.Ripp-Baudot[10], O.Rohne[34], A.Romero[47], P.Ronchese[37], E.I.Rosenberg[1], P.Rosinsky[7], P.Roudeau[20], T.Rovelli[5], Ch.Royon[41], V.Ruhlmann-Kleider[41], A.Ruiz[42], H.Saarikko[16], Y.Sacquin[41], A.Sadovsky[17], G.Sajot[15], J.Salt[51], D.Sampsonidis[12], M.Sannino[14], A.Savoy-Navarro[24], Ph.Schwemling[24], B.Schwering[54], U.Schwickerath[18], F.Scuri[48], P.Seager[21], Y.Sedykh[17], A.M.Segar[36], N.Seibert[18], R.Sekulin[38], G.Sette[14], R.C.Shellard[6], M.Siebel[54], L.Simard[41], F.Simonetto[37], A.N.Sisakian[17], G.Smadja[26], N.Smirnov[44], O.Smirnova[25], G.R.Smith[38], A.Sokolov[44], A.Sopczak[18], R.Sosnowski[53], T.Spassov[22], E.Spiriti[40], S.Squarcia[14], C.Stanescu[40], M.Stanitzki[18], K.Stevenson[36], A.Stocchi[20], J.Strauss[52], R.Strub[10], B.Stugu[4], M.Szczekowski[53], M.Szeptycka[53], T.Tabarelli[29], A.Taffard[23], F.Tegenfeldt[50], F.Terranova[29], J.Timmermans[32], N.Tinti[5], L.G.Tkatchev[17], M.Tobin[23], S.Todorova[9], A.Tomaradze[2], B.Tome[22], A.Tonazzo[9], L.Tortora[40], P.Tortosa[51], G.Transtromer[25], D.Treille[9], G.Tristram[8], M.Trochimczuk[53], C.Troncon[28], M-L.Turluer[41], I.A.Tyapkin[17], P.Tyapkin[25],

S.Tzamarias[12], O.Ullaland[9], V.Uvarov[44], G.Valenti[9,5], E.Vallazza[48], P.Van Dam[32], W.Van den Boeck[2], J.Van Eldik[9,32], A.Van Lysebetten[2], N.van Remortel[2], I.Van Vulpen[32], G.Vegni[28], L.Ventura[37], W.Venus[38,9], F.Verbeure[2], P.Verdier[26], M.Verlato[37], L.S.Vertogradov[17], V.Verzi[28], D.Vilanova[41], L.Vitale[48], E.Vlasov[44], A.S.Vodopyanov[17], G.Voulgaris[3], V.Vrba[13], H.Wahlen[54], C.Walck[46], A.J.Washbrook[23], C.Weiser[9], D.Wicke[9], J.H.Wickens[2], G.R.Wilkinson[36], M.Winter[10], M.Witek[19], G.Wolf[9], J.Yi[1], O.Yushchenko[44], A.Zalewska[19], P.Zalewski[53], D.Zavrtanik[45], E.Zevgolatakos[12], N.I.Zimin[17,25], A.Zintchenko[17], Ph.Zoller[10], G.C.Zucchelli[46], G.Zumerle[37]

[1]Department of Physics and Astronomy, Iowa State University, Ames IA 50011-3160, USA
[2]Physics Department, Univ. Instelling Antwerpen, Universiteitsplein 1, B-2610 Antwerpen, Belgium
and IIHE, ULB-VUB, Pleinlaan 2, B-1050 Brussels, Belgium
and Faculté des Sciences, Univ. de l'Etat Mons, Av. Maistriau 19, B-7000 Mons, Belgium
[3]Physics Laboratory, University of Athens, Solonos Str. 104, GR-10680 Athens, Greece
[4]Department of Physics, University of Bergen, Allégaten 55, NO-5007 Bergen, Norway
[5]Dipartimento di Fisica, Università di Bologna and INFN, Via Irnerio 46, IT-40126 Bologna, Italy
[6]Centro Brasileiro de Pesquisas Físicas, rua Xavier Sigaud 150, BR-22290 Rio de Janeiro, Brazil
and Depto. de Física, Pont. Univ. Católica, C.P. 38071 BR-22453 Rio de Janeiro, Brazil
and Inst. de Física, Univ. Estadual do Rio de Janeiro, rua São Francisco Xavier 524, Rio de Janeiro, Brazil
[7]Comenius University, Faculty of Mathematics and Physics, Mlynska Dolina, SK-84215 Bratislava, Slovakia
[8]Collège de France, Lab. de Physique Corpusculaire, IN2P3-CNRS, FR-75231 Paris Cedex 05, France
[9]CERN, CH-1211 Geneva 23, Switzerland
[10]Institut de Recherches Subatomiques, IN2P3 - CNRS/ULP - BP20, FR-67037 Strasbourg Cedex, France
[11]Now at DESY-Zeuthen, Platanenallee 6, D-15735 Zeuthen, Germany
[12]Institute of Nuclear Physics, N.C.S.R. Demokritos, P.O. Box 60228, GR-15310 Athens, Greece
[13]FZU, Inst. of Phys. of the C.A.S. High Energy Physics Division, Na Slovance 2, CZ-180 40, Praha 8, Czech Republic
[14]Dipartimento di Fisica, Università di Genova and INFN, Via Dodecaneso 33, IT-16146 Genova, Italy
[15]Institut des Sciences Nucléaires, IN2P3-CNRS, Université de Grenoble 1, FR-38026 Grenoble Cedex, France
[16]Helsinki Institute of Physics, HIP, P.O. Box 9, FI-00014 Helsinki, Finland
[17]Joint Institute for Nuclear Research, Dubna, Head Post Office, P.O. Box 79, RU-101 000 Moscow, Russian Federation
[18]Institut für Experimentelle Kernphysik, Universität Karlsruhe, Postfach 6980, DE-76128 Karlsruhe, Germany
[19]Institute of Nuclear Physics and University of Mining and Metalurgy, Ul. Kawiory 26a, PL-30055 Krakow, Poland
[20]Université de Paris-Sud, Lab. de l'Accélérateur Linéaire, IN2P3-CNRS, Bât. 200, FR-91405 Orsay Cedex, France
[21]School of Physics and Chemistry, University of Lancaster, Lancaster LA1 4YB, UK
[22]LIP, IST, FCUL - Av. Elias Garcia, 14-1^{o}, PT-1000 Lisboa Codex, Portugal
[23]Department of Physics, University of Liverpool, P.O. Box 147, Liverpool L69 3BX, UK
[24]LPNHE, IN2P3-CNRS, Univ. Paris VI et VII, Tour 33 (RdC), 4 place Jussieu, FR-75252 Paris Cedex 05, France
[25]Department of Physics, University of Lund, Sölvegatan 14, SE-223 63 Lund, Sweden
[26]Université Claude Bernard de Lyon, IPNL, IN2P3-CNRS, FR-69622 Villeurbanne Cedex, France
[27]Univ. d'Aix - Marseille II - CPP, IN2P3-CNRS, FR-13288 Marseille Cedex 09, France
[28]Dipartimento di Fisica, Università di Milano and INFN-MILANO, Via Celoria 16, IT-20133 Milan, Italy
[29]Dipartimento di Fisica, Univ. di Milano-Bicocca and INFN-MILANO, Piazza delle Scienze 2, IT-20126 Milan, Italy
[30]Niels Bohr Institute, Blegdamsvej 17, DK-2100 Copenhagen Ø, Denmark
[31]IPNP of MFF, Charles Univ., Areal MFF, V Holesovickach 2, CZ-180 00, Praha 8, Czech Republic
[32]NIKHEF, Postbus 41882, NL-1009 DB Amsterdam, The Netherlands
[33]National Technical University, Physics Department, Zografou Campus, GR-15773 Athens, Greece
[34]Physics Department, University of Oslo, Blindern, NO-1000 Oslo 3, Norway
[35]Dpto. Fisica, Univ. Oviedo, Avda. Calvo Sotelo s/n, ES-33007 Oviedo, Spain
[36]Department of Physics, University of Oxford, Keble Road, Oxford OX1 3RH, UK
[37]Dipartimento di Fisica, Università di Padova and INFN, Via Marzolo 8, IT-35131 Padua, Italy
[38]Rutherford Appleton Laboratory, Chilton, Didcot OX11 OQX, UK
[39]Dipartimento di Fisica, Università di Roma II and INFN, Tor Vergata, IT-00173 Rome, Italy
[40]Dipartimento di Fisica, Università di Roma III and INFN, Via della Vasca Navale 84, IT-00146 Rome, Italy
[41]DAPNIA/Service de Physique des Particules, CEA-Saclay, FR-91191 Gif-sur-Yvette Cedex, France
[42]Instituto de Fisica de Cantabria (CSIC-UC), Avda. los Castros s/n, ES-39006 Santander, Spain
[43]Dipartimento di Fisica, Università degli Studi di Roma La Sapienza, Piazzale Aldo Moro 2, IT-00185 Rome, Italy
[44]Inst. for High Energy Physics, Serpukov P.O. Box 35, Protvino, (Moscow Region), Russian Federation
[45]J. Stefan Institute, Jamova 39, SI-1000 Ljubljana, Slovenia and Laboratory for Astroparticle Physics,
Nova Gorica Polytechnic, Kostanjeviska 16a, SI-5000 Nova Gorica, Slovenia,
and Department of Physics, University of Ljubljana, SI-1000 Ljubljana, Slovenia
[46]Fysikum, Stockholm University, Box 6730, SE-113 85 Stockholm, Sweden
[47]Dipartimento di Fisica Sperimentale, Università di Torino and INFN, Via P. Giuria 1, IT-10125 Turin, Italy
[48]Dipartimento di Fisica, Università di Trieste and INFN, Via A. Valerio 2, IT-34127 Trieste, Italy
and Istituto di Fisica, Università di Udine, IT-33100 Udine, Italy
[49]Univ. Federal do Rio de Janeiro, C.P. 68528 Cidade Univ., Ilha do Fundão BR-21945-970 Rio de Janeiro, Brazil
[50]Department of Radiation Sciences, University of Uppsala, P.O. Box 535, SE-751 21 Uppsala, Sweden
[51]IFIC, Valencia-CSIC, and D.F.A.M.N., U. de Valencia, Avda. Dr. Moliner 50, ES-46100 Burjassot (Valencia), Spain
[52]Institut für Hochenergiephysik, Österr. Akad. d. Wissensch., Nikolsdorfergasse 18, AT-1050 Vienna, Austria
[53]Inst. Nuclear Studies and University of Warsaw, Ul. Hoza 69, PL-00681 Warsaw, Poland
[54]Fachbereich Physik, University of Wuppertal, Postfach 100 127, DE-42097 Wuppertal, Germany

1 Introduction

1.1 The R-parity violating Lagrangian

The most general way to write a superpotential, including the symmetries and particle content of the Minimal Supersymmetric extension of the Standard Model (MSSM) [1] is:

$$W = W_{MSSM} + W_{RPV} \tag{1}$$

where W_{MSSM} represents interactions between MSSM particles consistent with $B - L$ conservation (B = baryon number, L = lepton number) and W_{RPV} describes interactions violating B or L conservation [2]. This latter term of the superpotential can explicitly be written as[1] [3]:

$$\lambda_{ijk} L_i L_j \bar{E}_k + \lambda'_{ijk} L_i Q_j \bar{D}_k + \lambda''_{ijk} \bar{U}_i \bar{D}_j \bar{D}_k \tag{2}$$

where i, j and k are the generation indices; L and $\bar{E}$ denote the left-handed doublet lepton and the right-handed singlet charge-conjugated lepton superfields respectively, whereas Q, $\bar{U}$ and $\bar{D}$ denote the left-handed doublet quark and the right-handed singlet charge-conjugated up- and down-type quark superfields; λ_{ijk}, λ'_{ijk} and λ''_{ijk} are the Yukawa couplings. The first two terms violate L conservation, and the third term B conservation. Since $\lambda_{ijk} = -\lambda_{jik}$, $\lambda''_{ijk} = -\lambda''_{ikj}$, there are 9 λ_{ijk}, 27 λ'_{ijk} and 9 λ''_{ijk} leading to 45 additional couplings.

One major phenomenological consequence of R-parity violation ($\not{R}_p$) is that the Lightest Supersymmetric Particle (LSP) is allowed to decay into standard fermions. This fact modifies the signatures of the supersymmetric particle production compared to the expected signatures in case of R-parity conservation. First, the LSP may be a charged sparticle, for example a chargino (this case is considered in this paper). Second, due to the LSP decay into fermions, multi-lepton and multi-jet topologies are expected. In this paper, searches for pair produced neutralinos ($\widetilde{\chi}_i^0$), charginos ($\widetilde{\chi}^{\pm}$) and squarks ($\tilde{q}$) were performed under the hypothesis of R-parity violation with one single dominant $\bar{U}\bar{D}\bar{D}$ coupling. The $\bar{U}\bar{D}\bar{D}$ terms couple squarks to quarks and the experimental signature of the $\not{R}_p$ events thus becomes multiple hadronic jets, in most of the cases without missing energy. These signatures with R-parity violation through $\bar{U}\bar{D}\bar{D}$ terms have been already performed by the other LEP2 experiments [5].

1.2 Pair production of gauginos and squarks

Pair production of supersymmetric particles in MSSM with $\not{R}_p$ is the same as R_p conserved pair production, since the $\bar{U}\bar{D}\bar{D}$ couplings are not present in the production vertex.

The mass spectrum and the pair production cross sections of neutralinos and charginos are fixed, in the analyses described in this paper, by the three parameters of the MSSM theory assuming GUT scale unification of gaugino masses: M_2, the SU(2) gaugino mass parameter at the electroweak scale, μ, the mixing mass term of the Higgs doublets at the electroweak scale and $tan\beta$, the ratio of the vacuum expectation values of the two Higgs doublets. The cross section depends also on the common scalar mass at the GUT scale, m_0, due to selectron or sneutrino exchange in the t-channel for sufficiently low sfermions masses.

Pair production of squarks ($\tilde{q}$) is also studied in this paper. Here the cross-section mainly depends on the squark masses. In the case of the third generation, the left-right

[1] An additional fourth term in eq.2, describing a bilinear coupling between the left handed lepton superfield and the up-type Higgs field, is assumed to be zero [4].

mixing angle enters in the production cross-section as well. In the squark analysis two cases are considered: one with no mixing, the second with the mixing angle which gives the lowest production cross-section.

1.3 Direct and indirect decays of gauginos and squarks

The decay of the produced sparticles can either be direct or indirect. In a *direct decay* the sparticle decays directly or via a virtual sparticle exchange to standard particles through an $\not{R}_p$ vertex. In an *indirect decay* the sparticle first decays through an R_p conserving vertex to a standard particle and an on-shell sparticle, which then decays through an $\not{R}_p$ vertex. The squark analysis is done considering only the indirect decay channels which are dominant for coupling values considered in the present studies.

Figure 1 shows the direct and indirect decays of gauginos and the indirect decay of a squark via $\bar{U}\bar{D}\bar{D}$ couplings.

The most important features of these decays are the number of quarks in the final state which goes up to 10 for the indirect decay of two charginos. Table 1 displays the different event topologies from direct and indirect decays through $\bar{U}\bar{D}\bar{D}$ couplings of different pair produced sparticles. The 6-, 8-, 10-jet topologies of table 1 correspond to the decay diagrams in figure 1.

final states	direct decay of	indirect decay of
$4j$	$\widetilde{q}\widetilde{q}$	
$6j$	$\widetilde{\chi}_1^0\widetilde{\chi}_1^0$, $\widetilde{\chi}_2^0\widetilde{\chi}_1^0$, $\widetilde{\chi}_1^+\widetilde{\chi}_1^-$	
$8j$		$\widetilde{q}\widetilde{q}$
$10j$		$\widetilde{\chi}_1^+\widetilde{\chi}_1^-$

Table 1: The multijet final states in neutralino, chargino and squark pair production when one $\bar{U}\bar{D}\bar{D}$ coupling is dominant. The leptonic decays of W^* are not listed in these final states since only pure hadronic events are considered in this study.

1.4 $\bar{U}\bar{D}\bar{D}$ Couplings

The $\bar{U}\bar{D}\bar{D}$ Yukawa coupling strength, corresponding to a squark decay into two quarks, can be bound from above by indirect limits.

Upper limits on $\bar{U}\bar{D}\bar{D}$ couplings come from Standard Model constraints with experimental measurements:

- double nucleon decays for λ''_{112} couplings [6],
- $n-\bar{n}$ oscillations for λ''_{113} [7],
- $R_l = \Gamma_{had}(Z^0)/\Gamma_l(Z^0)$ for $\lambda''_{312}, \lambda''_{313}, \lambda''_{323}$ [8,9].

The upper limits on the other λ'' couplings do not come from experimental bounds. They are obtained from the requirement of perturbative unification at the GUT scale of 10^{16} GeV. This gives a limit of 1.25 for a sfermion mass of 100 GeV [6,10]. Upper limits on the $\bar{U}\bar{D}\bar{D}$ couplings are reported in table 2.

Our analysis, which does not search for long lived sparticles in the detector (displaced vertices), has a limited sensitivity to weak coupling strengths. The coupling strength

ijk	λ''_{ijk}	ijk	λ''_{ijk}	ijk	λ''_{ijk}
$\lambda''_{uds}(112)$	10^{-6}	$\lambda''_{cds}(212)$	1.25	$\lambda''_{tds}(312)$	0.43
$\lambda''_{udb}(113)$	10^{-5}	$\lambda''_{cdb}(213)$	1.25	$\lambda''_{tdb}(313)$	0.43
$\lambda''_{usb}(123)$	1.25	$\lambda''_{csb}(223)$	1.25	$\lambda''_{tsb}(323)$	0.43

Table 2: Upper limits on the $\bar{U}\bar{D}\bar{D}$ Yukawa couplings in units of ($m_{\tilde{f}}$/100 GeV), where $m_{\tilde{f}}$ is the appropriate squark mass [4].

dependence of the mean decay length of the LSP is given by [11,12]:

$$L(\mathrm{cm}) = 0.1\ (\beta\gamma) \left(\frac{\mathrm{m_{\tilde{f}}}}{100\ \mathrm{GeV}}\right)^4 \left(\frac{1\ \mathrm{GeV}}{\mathrm{m_{\widetilde{\chi}}}}\right)^5 \frac{1}{\lambda''^2} \tag{3}$$

if the neutralino or the chargino is the LSP with $\beta\gamma = P_{\widetilde{\chi}}/m_{\widetilde{\chi}}$. The typical lower limit of sensitivity for this analysis ($L \lesssim 1$ cm) is of the order of 10^{-4} (10^{-3}) in case of a $\widetilde{\chi}^0$or a $\widetilde{\chi}^{\pm}$ of 30 GeV (10 GeV), with a squark mass of 100 GeV.

For the generation of all the signals a λ''_{212} coupling of the strength 0.1 was used. A different choice between 10^{-2} and 0.5 would not change the neutralino decay topologies. The choice of this specific coupling was arbitrary, since all the analyses in this paper were coupling independent. Searches for decays through specific λ'' couplings, leading to the production of one or several b quarks, may indeed use the advantage of b-tagging techniques to reach higher sensitivities, but at the cost of lost generality. The aim of this paper was instead to perform a general coupling independent analysis for each of the search channels.

2 Data and MC samples

The analysis was performed on the data corresponding to an integrated luminosity of 158 pb^{-1} collected during 1998 by the DELPHI detector [13] at centre-of-mass energies around 189 GeV.

The contributions to the background coming from the Standard Model processes: four-fermion final states (WW, ZZ) and Z$\gamma\rightarrow q\bar{q}(\gamma)$ were considered. The contribution from $\gamma\gamma$ events after preselection was found to be negligible, due to the high detected energy fraction and multiplicities of the studied signals. For the Z$\gamma\rightarrow q\bar{q}\gamma$ backgrounds, the PYTHIA [14] generator was used whereas the four-fermion final states were generated with EXCALIBUR [15].

To evaluate signal efficiencies, sparticle production was generated using SUSYGEN [16]. All generated signal and background events were processed with the DELPHI detector simulation program (DELSIM).

3 Analyses

3.1 Topologies and analysis strategy

The present study covers the search for $\widetilde{\chi}^0_1$, $\widetilde{\chi}^+_1$and $\widetilde{q}$ pair production. The analysis of the different decay channels can be organized on the basis of the number of hadronic jets in the final state.

For each multijet analysis, the clustering of hadronic jets was performed by the *ckern* package[17] based on the Cambridge clustering algorithm[18]. The choice of this clustering algorithm was motivated by its good performance for configurations with a mixture of soft and hard jets, the expected case for $\bar{U}\bar{D}\bar{D}$ events. Moreover, the algorithm provides a good resolution for the jet substructure which is present in $\bar{U}\bar{D}\bar{D}$ indirect decays. For each event, *ckern* provides all possible configurations between two and ten jets. The value of the variable y_{i+1} (for i between 1 and 9), that is the transition value of the DURHAM resolution variable y_{cut} for a given i, which changes the characterization of an event from an i to an $i+1$ jet configuration, constitutes a powerful tool to identify the topologies in multijet signals.

A neural network method was applied in order to distinguish signals from Standard Model background events. The SNNS [19] package was used for the training and validation of the neural networks. The training was done on samples of simulated background and signal. The exact configuration and input variables of each neural network depended on the search channel. Each neural network provided a discriminant variable which was used to select the final number of candidate events for each analysis.

3.2 Hadronic preselection

Preselection of pure hadronic events was performed at the starting point of the gaugino and squark analyses.

The following preselection criteria were applied for the gaugino (squark) analyses:

- the charged multiplicity had to be greater or equal to 15 (20);
- the total energy from charged particles was required to be greater than $0.30 \times \sqrt{s}$,
- the total energy was required to be greater than $0.55\ (0.53) \times \sqrt{s}$,
- the total energy from neutral particles was required to be less than $0.50\ (0.47) \times \sqrt{s}$.

With these preselections most of the $\gamma\gamma$ background was suppressed. Tighter requirements on charged multiplicity included in each analysis made this background negligible. Therefore in what follows the main background events will be the four-fermion events like $W^+W^-$and the $Z\gamma$ QCD events with hard gluon radiation. Signal efficiency at the level of hadronic preselection was between 80% and 90% for high and medium mass of pair-produced sparticles. The preselection efficiency for the lowest neutralino mass was around 70%. After the hadronic gaugino preselection the agreement between the number of observed events (4722) in data and the number of expected events (4736) from SM processes was rather good. Figure 2 shows the distributions of several variables after this hadronic preselection.

3.3 Charginos and neutralinos, 6- and 10-jet analyses

To be efficient for all possible neutralino and chargino masses, the 6- (10-) jet analysis was divided into 3 (2) different mass windows.

The signal selection in both channels was performed in two steps. First, we applied soft sequential criteria against mainly $Z\gamma$ QCD events, except in the case of the low neutralino mass window:

- the effective centre-of-mass energy had to be greater than 150 GeV,
- the energy of the most energetic photon had to be less than 30 GeV,
- the sphericity had to be greater than 0.05, the thrust lower than 0.92 and -log(y_3) was required to be lower than 6.

Thereafter, a neural network method was used to select the signal against the Zγ QCD and the four-fermion backgrounds. For each analysis window a specific neural network was trained. Topological variables used as inputs to the network were:

- oblateness,
- -log(y_n) with n=4 to 10,
- minimum di-jet mass in 4-, 5- and 6-jet configurations,
- energy of the least energetic jet $\times$ minimum di-jet angle in 4 and 5 jet configurations.

The training was performed in a standard back-propagation manner using the SNNS package [19]. The network configuration had 13 input nodes, 13 hidden nodes and 3 output nodes. The 3 output nodes correspond to the signal, the Zγ background and the four-fermion background. This choice was motivated by the fact that we were looking for different signal topologies which were either similar to Zγ or to four-fermion events depending on the analysis window.

3.3.1 Direct decay of $\widetilde{\chi}_1^0\widetilde{\chi}_1^0$ or $\widetilde{\chi}_1^+\widetilde{\chi}_1^-$ into 6 jets

The 6-jet analysis was divided into 3 mass windows to take into account the magnitude of the gaugino boost depending on its mass:

- window N1; low gaugino mass: $10 \leq m_{\tilde{\chi}} \leq 30$ GeV,
- window N2; medium gaugino mass: $30 < m_{\tilde{\chi}} \leq 70$ GeV,
- window N3; high gaugino mass: $70 < m_{\tilde{\chi}} \leq 94$ GeV.

The comparison between the number of expected SM background and the number of data events was performed for all neural network output values as is shown in Figure 3 for the medium gaugino N2 mass analysis window. Signal efficiencies were calculated only from signal validation events (signal training events were not used at this level) for each neural network output value. Then the expected and obtained number of data events as a function of the signal efficiency was plotted as for example in Figure 4 for the N2 analysis window.

No excess in the data appeared in these distributions, therefore a working point optimization on the neural network output was performed minimizing the expected excluded cross-section as a function of the average signal efficiency of the mass window. The working points of the neural network output were 0.953, 0.852 and 0.966 for mass windows N1, N2 and N3 respectively. The corresponding signal efficiencies which increase with the neutralino mass were around 10-15%, 25-30% and 20-30% for the mass windows N1, N2 and N3 respectively. To obtain signal efficiencies, the full detector simulation was performed on neutralino pair production with a 10 GeV step grid in the neutralino mass (10 to 94 GeV). The statistical errors on the efficiencies was typically 2%.

No excess of data over background was observed for any working point. The numbers of events seen and expected from backgrounds are shown in table 3.

3.3.2 Indirect decay of $\widetilde{\chi}_1^+\ \widetilde{\chi}_1^-$ into 10 jets

The 10-jet analysis was more sensitive to the mass difference between the chargino and the neutralino than to the neutralino mass. To take into account this mass difference we divided the 10-jet analysis into 2 windows:

- window C1; low chargino neutralino mass difference: $\Delta M \leq 10$ GeV,
- window C2; high chargino neutralino mass difference: $\Delta M > 10$ GeV.

Window	Data	backgrounds	Zγ background	four-fermion backgrounds
N1	13	11.5 $\pm$ 0.4	10	1.5
N2	25	23.8 $\pm$ 0.5	2.6	21.2
N3	9	6.3 $\pm$ 0.3	0.4	5.9

Table 3: The numbers of events seen and expected from backgrounds for the three mass windows of the 6-jet analysis.

The same neural network method was applied to select 10-jet events coming from indirect chargino decays. Two neural networks for the two different windows were produced. The distributions from expected SM events and data events were in good agreement. The neural network output of the C2 mass analysis is given in Figure 5 as an example. Figure 6 shows the number of expected events and data events as a function of the signal efficiency for the C2 mass window.

The optimal working points have been found with the same procedure as for the 6-jet analysis. The neural network output values were 0.894 and 0.956 for two mass windows (C1 and C2). The corresponding signal efficiencies were around 15-25% and 10-50% for the two mass windows. The statistical errors on the signal efficiency was 2%.

In Figure 6 it can be seen that the background is not perfectly reproduced by the simulation in the high efficiency region dominated by $Z\gamma$ background, i.e. at the preselection level. This region of high efficiency is not considered in the final signal selection which is in the 10%-50% efficiency region. The signal region is mainly dominated by four-fermion background. Therefore, an increase of the uncertainty of the $Z\gamma$ background does not drastically affect the uncertainty on the expected background in the vicinity of the working point.

No excess was found in observed events compared to expected background for any working point. The numbers of events seen and expected from backgrounds are shown in table 4.

Window	Data	backgrounds	Zγ background	four-fermion backgrounds
C1	28	25.3 $\pm$ 0.6	3.1	22.2
C2	18	21.0 $\pm$ 0.5	1.8	19.3

Table 4: The numbers of events seen and expected from backgrounds for the three mass windows of the 10-jet analysis.

3.4 Squark 8-jet analysis

Searches for squarks were performed in the case of indirect decays through a dominant R-parity violating $\bar{U}\bar{D}\bar{D}$ coupling. The final states in the indirect decay channel contain eight quarks of any flavour, but the topology of the signal strongly depends on the mass of the $\widetilde{\chi}_1^0$, through which the decay proceeds. SUSY signals were therefore simulated at different squark masses in the range 50-90 GeV with $\widetilde{\chi}_1^0$ masses between 10-80 GeV. The simulated decay actually used for the studies and efficiency evaluation was $\widetilde{b} \rightarrow b\ \widetilde{\chi}_1^0$.

The general analysis methods based on a neural network background rejection were adopted for the analysis. The analysis was aimed at a good sensitivity for R-parity

violating $\bar{U}\bar{D}\bar{D}$ signals all over the plane of kinematically available squark and $\widetilde{\chi}_1^0$ masses. First a general preselection, in addition to the one presented in section 3.2, was made with the aim of a high general efficiency for the signal and at the same time a good rejection of low multiplicity hadronic background events. The selection criteria were optimized for the 8-jet squark analysis with the following variables:

- the energy of the most energetic photon in the event had to be less than 45 GeV,
- the missing momentum of the event had to be less than 76 GeV,
- the oblateness of the event had to be less than 0.5.

A neural network was thereafter trained to calculate a discriminant variable for each event, in order to distinguish a possible signal from Standard Model background. The following quantities were used as input to the neural network:

- the total energy from neutral particles, the total event energy, the total number of charged particles, the energy of the most energetic photon in the event, the missing momentum of the event, the oblateness of the event,
- -log(y_n) with $n = 2$ to 10,
- the reconstructed mass from a 5 constraint kinematic fit (the fifth constraint is the equal mass constraint on the di-jet masses) performed on the 4 jet topology of the event and the χ^2 value of this fit,
- the minimum angle between two jets times the minimum jet energy from the 5 jet topology of the event.

Note that some of the input variables for the neural network were also used for the preselection, i.e. the preselection was used to eliminate the signal free regions and thereby unnecessary background from the analysis, whereas the neural network served to discriminate the signal from the background, in the remaining regions with overlapping values of the variables. The final selection of candidate events was made based on the output value of the neural network. The working point optimization on the neural network output was performed minimizing the expected excluded cross-section as a function of the average signal efficiency of the mass window. No excess of data over Standard Model backgrounds was observed. The numbers of events seen and expected from backgrounds are shown in table 5.

Data	backgrounds	Zγ background	four-fermion backgrounds
22	18.4 $\pm$ 0.7	3.8	14.6

Table 5: The numbers of events seen and expected from backgrounds for the three mass windows of the 8-jet analysis.

The signal efficiency was evaluated at each of the 30 evenly distributed simulated points in the plane of squark and neutralino masses and interpolated in the regions between. Efficiencies for the signal after the final selection range from 10-20%, for small or large mass differences between squark and neutralino, up to 50% for medium mass differences. The statistical errors on signal efficiencies were typically 2%.

4 MSSM interpretation of the results

No excess was seen in the data with respect to the expected background in any of the channels of these analyses. Therefore, limits at 95% confidence level on the cross-section

of each process were obtained. Mass limits were derived for supersymmetric particles in the MSSM frame with $\not{R}_p$. The cross-section (σ_{95}) that can be excluded experimentally at 95% confidence level, was calculated from data and SM event numbers obtained at the end of each analysis [20].

4.1 Chargino and neutralino multi-jet searches

The excluded cross-sections, which is the σ_{95} divided by the signal efficiency, are in the range [0.5, 0.7] pb, [0.2, 0.3] pb and [0.3, 0.4] pb for the N1, N2 and N3 neutralino analysis mass windows respectively and in the range [0.3, 0.6] pb and [0.1, 0.2] pb for the C1 and C2 indirect chargino decay analysis mass windows.

The signal efficiency for any value of $\widetilde{\chi}_1^0$ and $\widetilde{\chi}^{\pm}$ masses was interpolated using an efficiency grid determined with signal samples produced with the full DELPHI detector simulation. For typical values of tanβ and m_0, a (μ,M_2) point was excluded at 95% confidence level if the signal cross-section times the efficiency at this point was greater than the cross-section (σ_{95}).

Adding the 6-jet analysis (used for the direct decay of $\tilde{\chi}_1^+\tilde{\chi}_1^-$ or $\tilde{\chi}_1^0\tilde{\chi}_1^0$) and the 10-jet analysis (used for indirect decay of $\tilde{\chi}_1^+\tilde{\chi}_1^-$) results, an exclusion contour in the μ, M_2 plane at 95% confidence level was derived for different values of m_0 (90 and 300 GeV) and tanβ (1.5 and 30). These exclusion contours in the μ, M_2 plane are shown in Figure 7. In the exclusion plots the main contribution comes from the study of the chargino indirect decays with the 10-jet analysis, due to the high cross-section. The 6-jet analysis becomes crucial in the exclusion plot for low tanβ value, low m_0 values and negative μ values. A 95 % CL lower limits on the mass of lightest neutralino and chargino are obtained from the μ, M_2 plane for different values of tan β between 0.5 and 30 and for $m_0 = 500$ GeV. The result on the lightest neutralino as a function of tanβ is shown in Figure 8. A lower limit on neutralino mass of 32 GeV is obtained. The chargino is mainly excluded up to the kinematic limit at 94 GeV.

4.2 Indirect squark multi-jet searches

Exclusion domains were obtained by calculating σ_{95} divided by the signal efficiency for each 1 GeV×1 GeV bin in the neutralino mass versus squark mass plane and comparing them to the cross-section for pair-produced squarks. The excluded cross-section varies between 0.2 and 0.9 pb depending on the efficiency. The resulting exclusion contours for stop and sbottom can be seen in Figure 9. A 100% branching ratio of indirect decays in the neutralino channel was assumed for this exclusion. The mixing angle 0.98 rad corresponds to the minimal lightest stop cross-section due to a maximal decoupling from the Z boson.

By combining the exclusion contours from the squark searches with the constraint on the neutralino mass from the gaugino searches, lower bounds on the squark masses with $\Delta M > 5$ GeV are achieved. The lower mass limit on the stop is 74 GeV in the case of no mixing, and 59 GeV in the case of maximal Z-decoupling. The lower mass limit on the sbottom is 72 GeV in the case of no mixing. For sbottom the minimum cross-section is too low to extract any exclusion with the present analysis.

5 Summary

Searches for pair-produced gauginos and squarks, in the case of a single dominant R-parity violating $\bar{U}\bar{D}\bar{D}$ coupling, were performed on data collected by the DELPHI detector at a centre-of-mass energy of 189 GeV. The analysis of the hadronic multijet final-states was performed by means of a neural network method and the results were interpreted within the framework of the MSSM. No excess of data over the expected Standard Model events was found in any of the investigated search channels. The result of the analysis implies the following lower mass limits, at a 95 % confidence level, on supersymmetric particles:

- neutralino mass: $m_{\tilde{\chi}_1^0} \geq 32$ GeV
- chargino mass: $m_{\tilde{\chi}_1^+} \geq 94$ GeV
- stop and sbottom mass (indirect decay) with $\Delta M > 5$ GeV:
  $m_{\tilde{t_1}} \geq 74$ GeV, for $\Phi_{mix} = 0$ rad
  $m_{\tilde{t_1}} \geq 59$ GeV, for $\Phi_{mix} = 0.98$ rad
  $m_{\tilde{b_1}} \geq 72$ GeV, for $\Phi_{mix} = 0$ rad.

These mass limits were obtained under the following assumptions :

- One $\bar{U}\bar{D}\bar{D}$ term is dominant.
- The limit on the neutralino and chargino masses were obtained for any m_0, tan β values and for $-200 < \mu < 200$ GeV and $0 < M_2 < 400$ GeV.
- The strength of the λ'' coupling was assumed to be greater than 10^{-3}, limited by a mean LSP decay length smaller than 1 cm. Smaller coupling strengths lead to a region between dominant R-parity violation and R-parity conservation, which is not covered by these analyses.
- stop and sbottom mass limits are valid for $\Delta M > 5$ GeV. They were obtained for μ = -200 GeV and tan $\beta = 1.5$. A branching ratio of 100 % into quark-neutralino was assumed.

Acknowledgements

We are greatly indebted to our technical collaborators, to the members of the CERN-SL Division for the excellent performance of the LEP collider, and to the funding agencies for their support in building and operating the DELPHI detector.
We acknowledge in particular the support of
Austrian Federal Ministry of Science and Traffics, GZ 616.364/2-III/2a/98,
FNRS–FWO, Belgium,
FINEP, CNPq, CAPES, FUJB and FAPERJ, Brazil,
Czech Ministry of Industry and Trade, GA CR 202/96/0450 and GA AVCR A1010521,
Danish Natural Research Council,
Commission of the European Communities (DG XII),
Direction des Sciences de la Matière, CEA, France,
Bundesministerium für Bildung, Wissenschaft, Forschung und Technologie, Germany,
General Secretariat for Research and Technology, Greece,
National Science Foundation (NWO) and Foundation for Research on Matter (FOM), The Netherlands,
Norwegian Research Council,
State Committee for Scientific Research, Poland, 2P03B06015, 2P03B1116 and SPUB/P03/178/98,
JNICT–Junta Nacional de Investigação Científica e Tecnológica, Portugal,
Vedecka grantova agentura MS SR, Slovakia, Nr. 95/5195/134,
Ministry of Science and Technology of the Republic of Slovenia,
CICYT, Spain, AEN96–1661 and AEN96-1681,
The Swedish Natural Science Research Council,
Particle Physics and Astronomy Research Council, UK,
Department of Energy, USA, DE–FG02–94ER40817.

The financial support of STINT, The Swedish Foundation for International Cooperation in Research and Higher Education, and NFR, The Swedish Natural Science Research Council, is highly appreciated.

References

[1] For reviews, see e.g. H.P. Nilles, Phys. Rep. 110 (1984) 1.
H.E. Haber and G.L. Kane, Phys. Rep. 117 (1985) 75.
[2] P. Fayet, Phys. Lett. B69 (1977) 489.
G. Farrar and P. Fayet, Phys. Lett. B76 (1978) 575.
[3] S. Weinberg, Phys. Rev. D26 (1982) 287.
[4] H. Dreiner, in 'Perspectives on Supersymmetry', Ed. by G.L. Kane, World Scientific, July 1997, 462-479 (hep-ph/9707435). .
[5] ALEPH Collaboration, R. Barate et al. *Eur. Phys. J.***C7** (1999) 383.
L3 Collaboration, M. Acciari et al. Phys. Lett. B459 (1999) 354.
OPAL Collaboration, G. Abbiendi *Eur. Phys. J.***C11** (1999) 619.
[6] J.L. Goity, Marc Sher, Phys. Lett. B346 (1995) 69.
erratum-ibid. B385 (1996) 500.
[7] F. Zwirner, Phys. Lett. B132 (1983) 103.
[8] G. Bhattacharyya, J. Ellis, K. Sridhar, *Mod. Phys. Lett.* **A10** (1995) 1583
.G. Bhattacharyya, D. Choudhury, K. Sridhar, Phys. Lett. B355 (1995) 193.

J. Ellis, S. Lola and K. Sridhar, Phys. Lett. B408 (1997) 252.

[9] G. Bhattacharyya, Nucl. Phys. Proc. Suppl. 52A (1997) 83.

[10] B. Brahmachari, Probir Roy, Phys. Rev. D50 (1994) 39.
erratum-ibid. D51 (1995) 3974.
[11] S. Dawson, Nucl. Phys. B261 (1985) 297.
[12] H. Dreiner and G.G. Ross, Nucl. Phys. B365 (1991) 597.
[13] P. Abreu et al., Nucl. Instr. Meth. A378 (1996) 57.
[14] T. Sjöstrand, Computer Phys. Comm. 39 (1986) 347.
[15] F.A. Berends, R. Kleiss, R. Pittau, Computer Phys. Comm. 85 (1995) 437.
[16] S. Katsanevas, P. Morawitz, Computer Phys. Comm. 112 (1998) 227.
[17] S. Bentvelsen and I. Meyer, *Eur. Phys. J.***C4** (1998) 623..
[18] Yu.L. Dokshitzer, G.D. Leder, S. Moretti, B.R. Webber, J. High Energy Phys. 08 (1997) 001.
[19] A. Zell et al., SNNS User manual, Version 4.1, Report N 6/95. SNNS is (c) (Copyright) 1990-95 SNNS Group, Institute for Parallel and Distributed High-Performance Systems (IPVR), University of Stuttgart, Breitwiesenstrasse 20-22, 70565 Stuttgart, Fed. Rep. of Germany.
[20] Particle Data Group, Phys. Rev. D54 (1996) 1.
F. James and M. Roos, Phys. Rev. D44 (1991) 299.

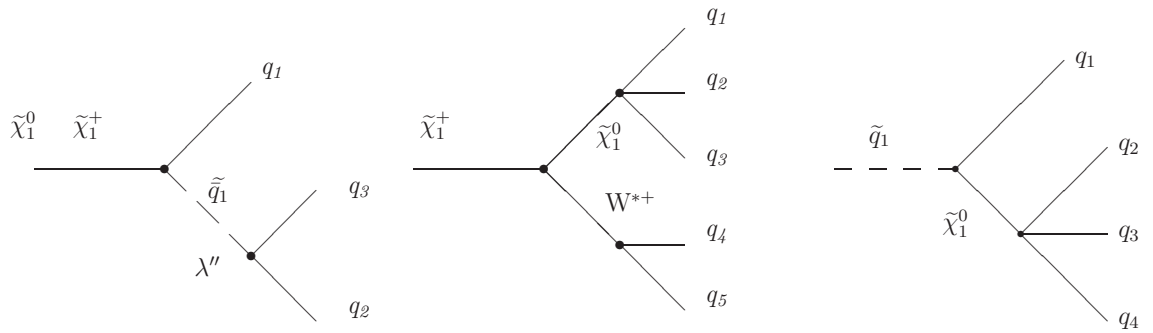

Figure 1: $\widetilde{\chi}_1^0$, $\widetilde{\chi}_1^+$ direct decay (left), $\widetilde{\chi}_1^+$ (center) and $\widetilde{q}$ (right) indirect decay with a dominant $\bar{U}\bar{D}\bar{D}$ coupling. W^{*+} is an off-shell W^+ boson.

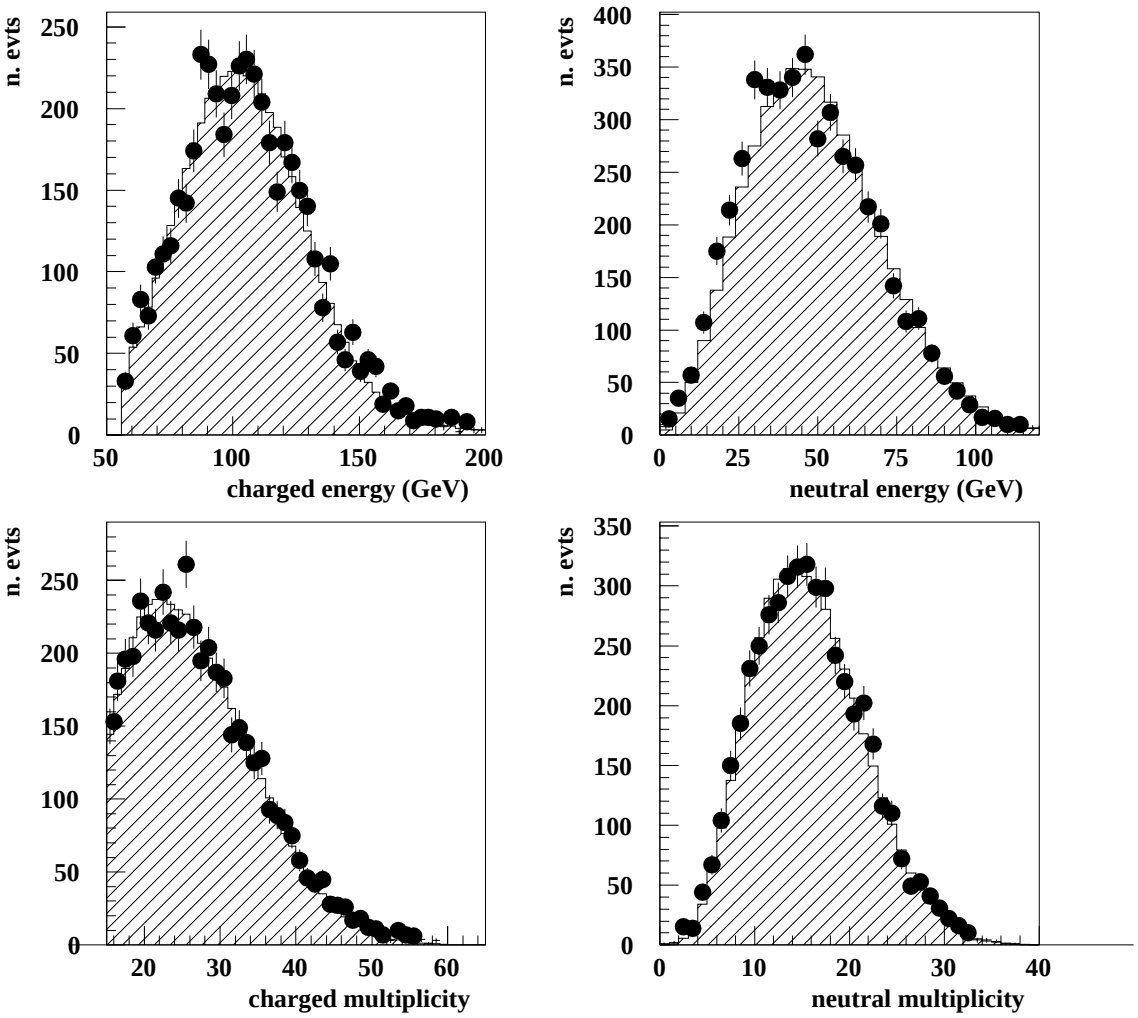

Figure 2: Charged (upper left), neutral (upper right) energy distributions and charged (lower left) and neutral (lower right) multiplicity distributions after hadronic preselection of gaugino analyses for data (black dots), expected SM background (hatched histograms).

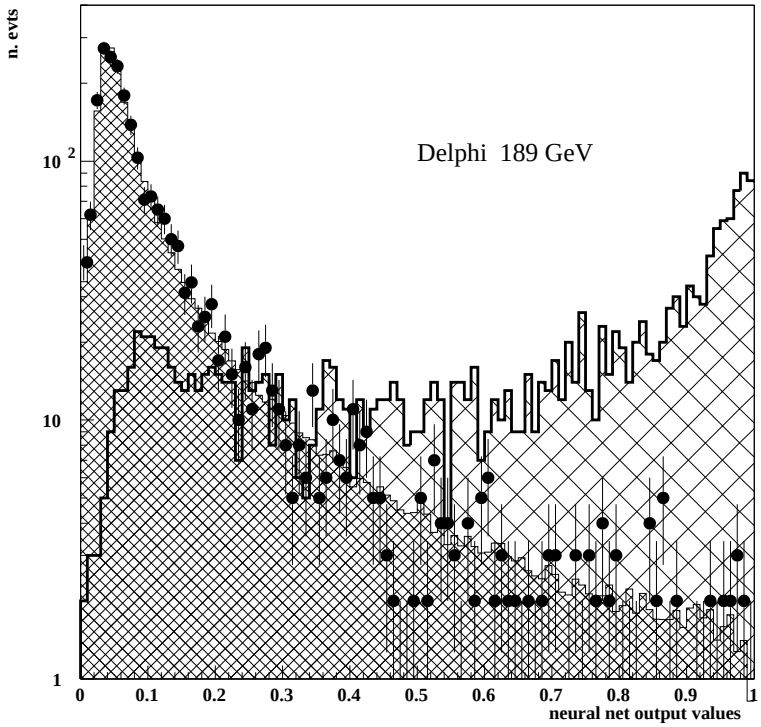

Figure 3: Neural network signal output for data (black dots), expected SM background (tight hatched) and the unweighted signals (loose hatched) corresponding to the medium gaugino mass search N2.

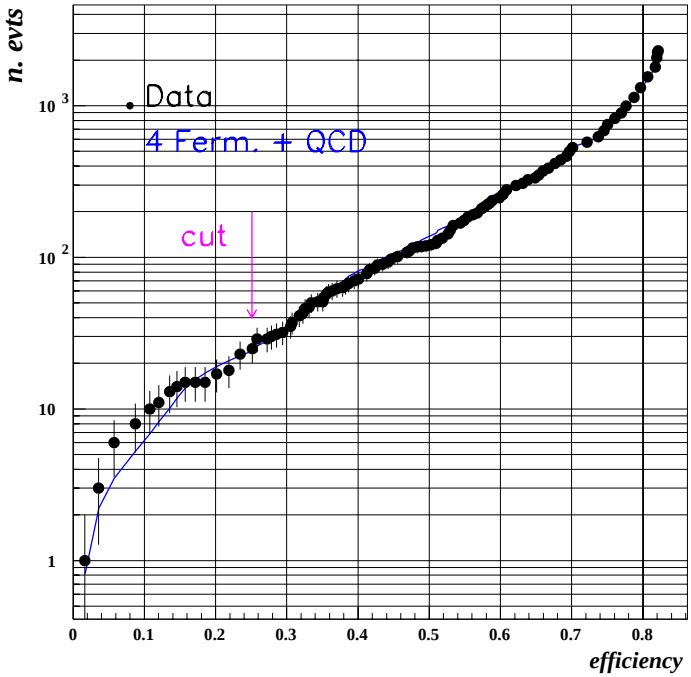

Figure 4: Number of expected events (continuous line) data events (black dots) versus signal efficiency for a 60 GeV neutralino mass in the medium gaugino mass search N2. The arrow shows the efficiency corresponding to the working point.

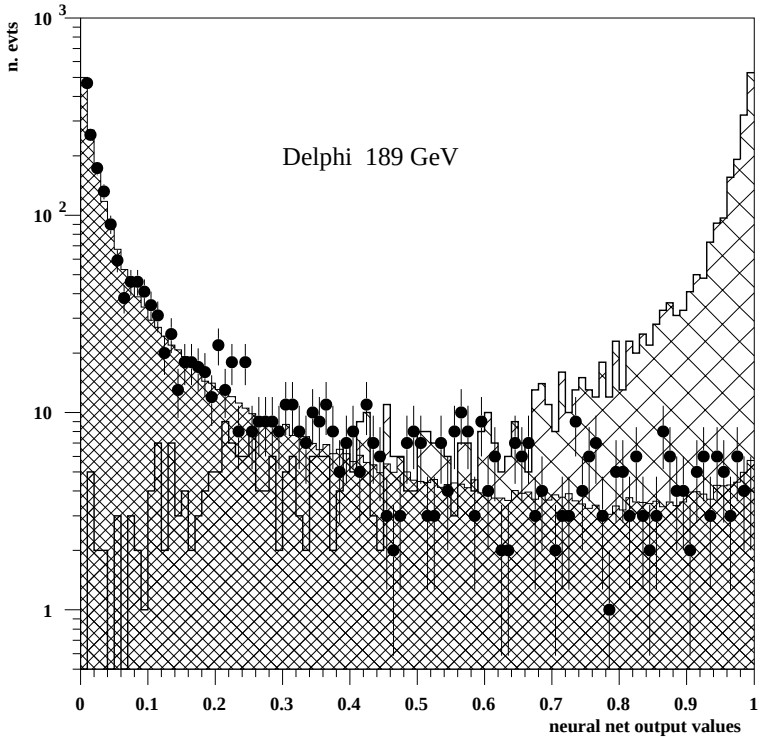

Figure 5: Neural network signal output for data (black dots), expected SM background (tight hatched) and the unweighted signals (loose hatched) corresponding to the analysis applied in case of large ΔM between chargino and neutralino (window C2).

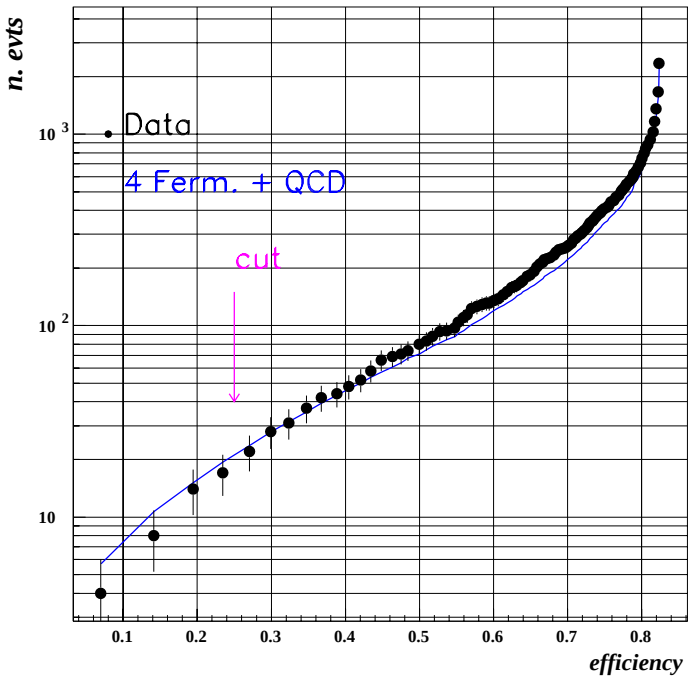

Figure 6: Number of expected events (continuous line) data events (black dots) versus signal efficiency for a chargino mass of 80 GeV and a neutralino mass of 50 GeV in the analysis applied in case of large ΔM between chargino and neutralino (window C2). The arrow shows the efficiency corresponding to the working point.

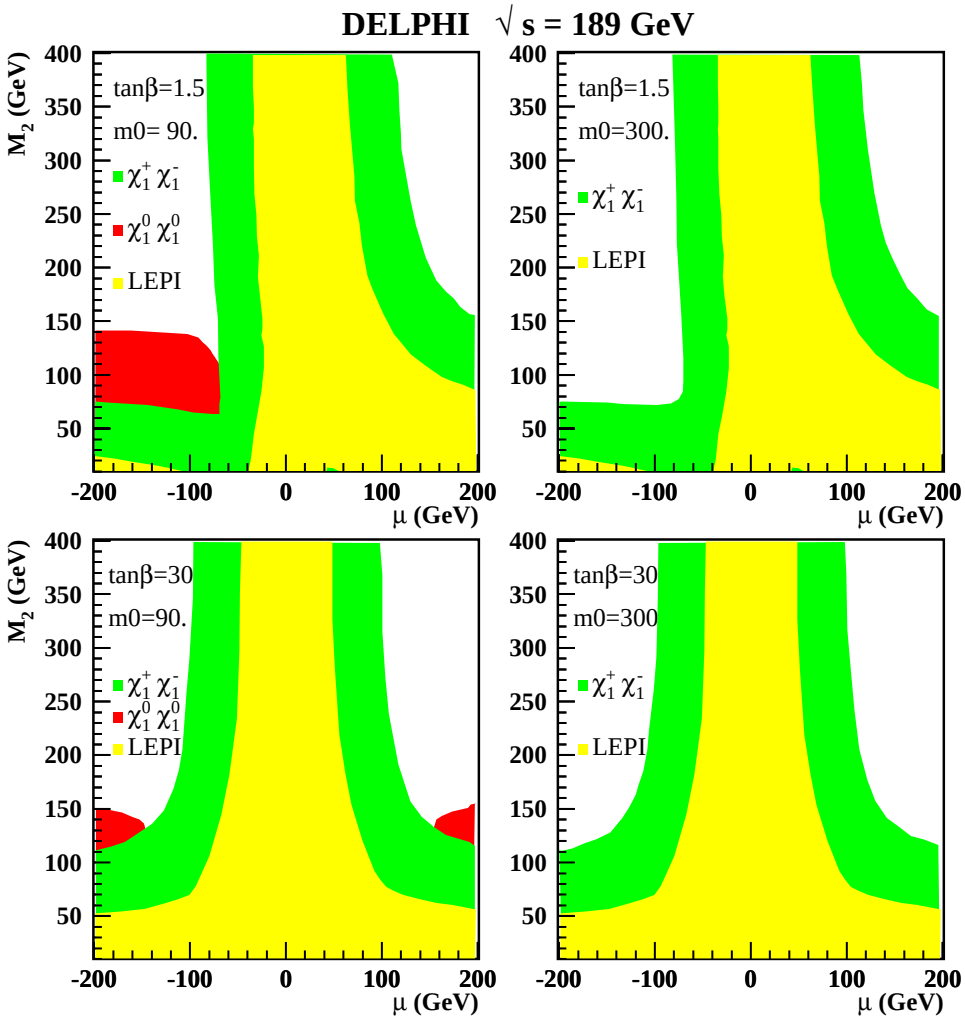

Figure 7: Exclusion plot in μ, M_2 plane for $\tilde{\chi}_1^0\ \tilde{\chi}_1^0$ and $\tilde{\chi}_1^+\ \tilde{\chi}_1^-$ production in the case of a dominant $\bar{U}\bar{D}\bar{D}$ R-parity violation coupling. The 6- and 10-jets analyses are treated separately for this exclusion. The shaded areas are excluded.

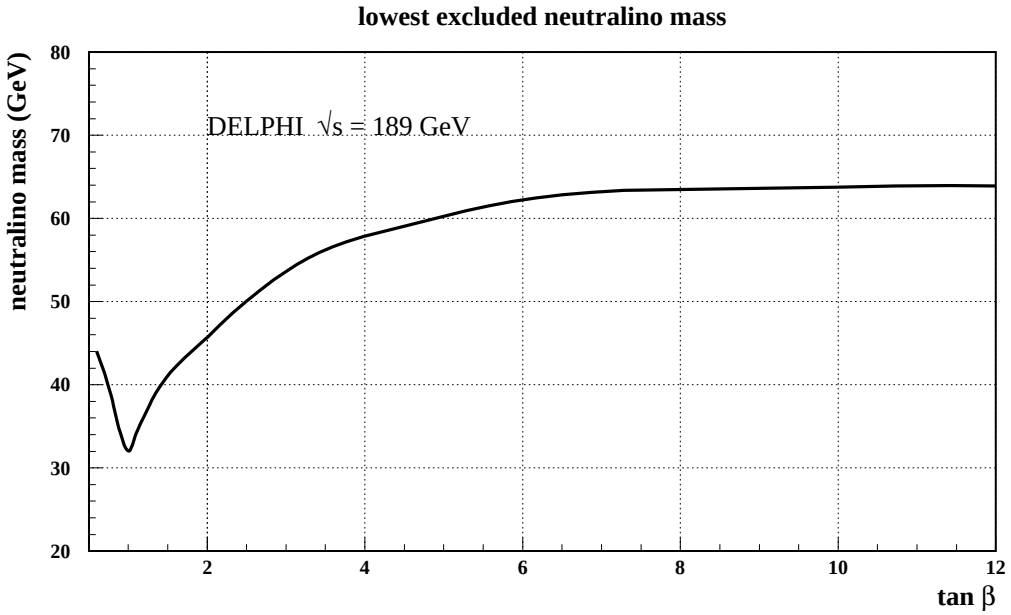

Figure 8: The excluded lightest neutralino mass as a function of tan β at 95% confidence level.

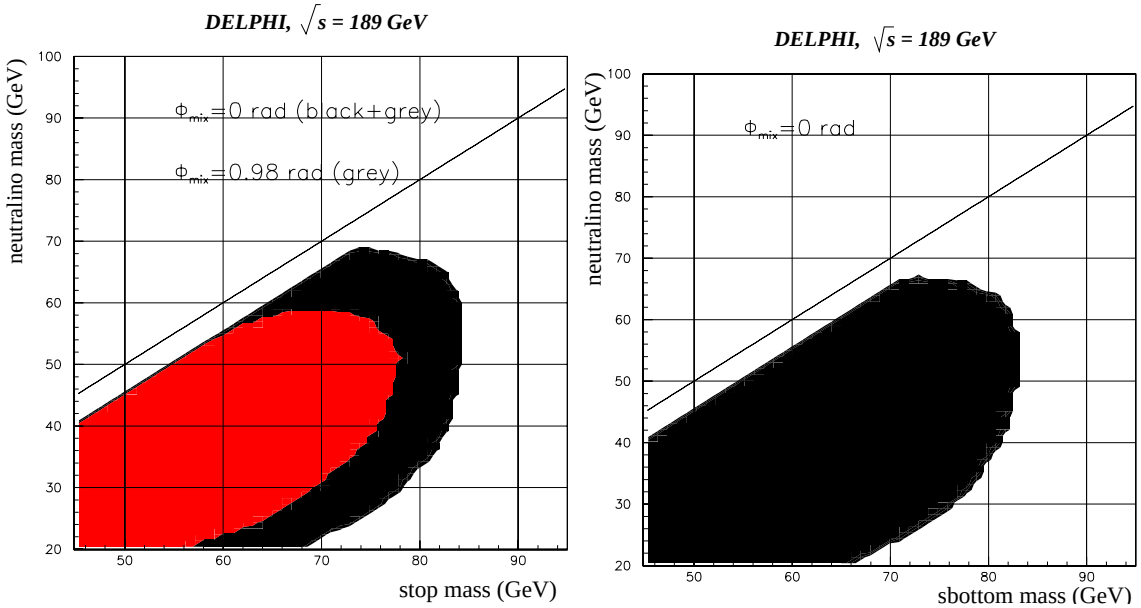

Figure 9: Exclusion domains at 95% confidence level in the $M(\tilde{\chi}_1^0)$, $M(\tilde{q})$ plane for indirect squark decays in the case of a 100 % branching ratio in the neutralino channel. The left plot shows the exclusion for a stop in the case of no mixing and with the mixing angle ϕ_{mix} which gives a minimum cross-section. For sbottom the minimum cross-section is too low to extract any exclusion with the present analysis. The diagonal lines indicate the degenerate mass limit above which indirect squark decays are forbidden.